26. Mortillaro, M. J. *et al.* A hyperphosphorylated form of the large subunit of RNA polymerase II is associated with splicing complexes and the nuclear matrix. *Proc. Natl Acad. Sci. USA* **93,** 8253–8257 (1996).
27. Kim, E., Du, L., Bregman, D. B. & Warren, S. L. Splicing factors associate with hyperphosphorylated RNA polymerase II in the absence of pre-mRNA *J. Cell Biol.* **136,** 19–28 (1997).
28. McCracken, S. *et al.* The C-terminal domain of RNA polymerase II couples mRNA processing to transcription. *Nature* **385,** 357–361 (1997).
29. Habets, W. J., Hoet, M. H., DeJong, B. A. W., VanDer Kemp, A. & Van Venrooij, W. J. Mapping of B cell epitopes on small nuclear ribonucleoproteins that react with human autoantibodies as well as with experimentally induced mouse monoclonal antibodies. *J. Immunol.* **143,** 2560–2466 (1986).

Supplementary information is available on *Nature*'s World-Wide Web site (http://www.nature.com) or from Mary Sheehan at the London editorial office of *Nature*.

Acknowledgements. We thank R. Dirks, D. Helfman, A. Krainer and T. Traavik for reagents; J. McCann for preparation of *in situ* hybridization probes; and T. Maniatis, A. Krainer and members of the Krainer and Spector labs for discussion and reading of the manuscript. T. M. was supported by the Human Frontiers Science Program fellowship and the Swiss National Science Foundation. Work in the laboratory of D.L.S. is supported by a grant from the NIH/NIGMS.

Correspondence and requests for materials should be addressed to D.L.S. (spector@cshl.org).

Dimeric association and segmental variability in the structure of human CD4

Hao Wu, Peter D. Kwong & Wayne A. Hendrickson*

*Department of Biochemistry and Molecular Biophysics and * Howard Hughes Medical Institute, Columbia University, New York, New York 10032, USA*

CD4 is a co-receptor in the cellular immune response. It increases the avidity of association between a T cell and an antigen-presenting cell by interacting with non-polymorphic portions of the complex between class II major histocompatibility complex (MHC) and T-cell receptor (TCR) molecules, and it contributes directly to signal transduction through its cytoplasmic association with the lymphocyte kinase Lck (ref. 1). CD4 also serves as the high-affinity receptor for cellular attachment and entry of the human immunodeficiency virus (HIV)[2]. The extracellular portion of CD4 comprises four immunoglobulin-like domains (D1–D4). This part of human CD4 (residues 1–369) has been characterized as a recombinant soluble protein (sCD4)[3,4], and crystal structures have been described for the human D1D2 fragment[5,6] and for the rat D3D4 fragment[7]. We have now determined the structures of intact sCD4 in three crystal lattices. These structures have a hinge-like variability at the D1D2 to D3D4 junction that might be important in immune recognition and HIV fusion, and a common dimeric association through D4 domains. Dynamic light scattering measurements and chemical crosslinking of sCD4 corroborate dimerization at high protein concentration. We suggest that such dimers may have relevance as mediators of signal transduction in T cells.

Crystals of sCD4 were grown as described previously[4] except we started from the selenomethionyl protein. Moreover, the extent of measurable diffraction was increased through cryoprotection. The structure of a tetragonal type-C crystal was determined by molecular replacement[8], confirmed by selenium Bijvoet-difference Fourier analyses, and refined with tight restraints at 3.9 Å resolution. This model was then used to solve the structures of selenomethionyl sCD4 in a new monoclinic type-F lattice and of native sCD4 in the trigonal type-A lattice. These structures were refined from rigid-body components only (Table 1). Although the results were obtained at modest resolution, they can be interpreted with confidence in light of the detailed structures of the component domains[7,9]. Density became resolved during refinement for the D1D2 to D3D4 connecting segment (residues 179–181) and for a carboxy-terminal extension (residues 362–363). These segments, as well as changes in sequence from rat to human D3D4 domain (58% identity), were modelled and refined. Residues 364–369 are not ordered in the crystals and may provide a flexible linkage to the transmembrane segment.

The six independent molecules in these crystals all have a similar extended structure (Fig. 1a), and in each crystal the two molecules per asymmetric unit are related by the same diad association of D4 domains (Fig. 1b). Lattice contacts elsewhere are distinctive (Fig. 1c), although one set of D1D2 contacts is similar in the tetragonal and monoclinic crystals. The D4–D4-associated dimers are butterfly-shaped in profile (Fig. 1c) with D1–D3 as 'wings', D4 pairs as the 'torso' and the C termini as 'legs', as if perching on a hypothetical membrane surface perpendicular to the diad axis. Each D1D2 fragment is a fixed entity at this resolution, as is each D3D4 dimer. There is, however, appreciable variability in the D1D2 to D3D4 junctions, which ranges up to 10.4° in orientational difference (Fig. 1d). The angle at the D1D2 to D3D4 junction is 140° (type-C molecule 1) as defined by the angle between the 'Cys-axes' (line through midpoints of canonical disulphide bonds or equivalents in neighbouring domains), and the D1D2 Cys-axis is 53° from the molecular diad axis and presumed membrane normal. The refined D3D4 component is very similar to the rat D3D4 model (1.07 and 0.96 Å r.m.s. deviations for Cα position in D3 and D4 with 5.4° relative difference in interdomain orientation).

The interface between D2 and D3 is formed almost exclusively by the AB loop of D2 and the FG loop of D3, both of which are more extended than their counterparts in D4 or D1, plus the connecting strand itself (Fig. 1a). There is 450 Å^2 of non-hydrated surface area buried from each domain into this interface, which is similar to the interfacial areas between D1 and D2 and between D3 and D4. Four hydrophobic residues (Leu 109, Leu 177, Leu 200 and Leu 283) dominate the interface. There is also an apparent hydrogen bond between Gln 112 and Gly 281. All of these are conserved residues. The last strand of D2 (G) continues directly into the first strand of D3 (A), but in a tortuous manner because of kinks in the A strand of D3 that switch the pairing from strand B initially to strand G later, as in most immunoglobulin-variable domains. The hinge flexibility at the junction is likely to be at residues Leu 177 and Ala 178 because Val 176 and Phe 179 are core elements of the D2 and D3 β-sandwiches, respectively. The junctional variability among the six sCD4 copies (Fig. 1d) is accommodated with little adjustment at the mostly hydrophobic interface; indeed, much larger movements toward more acute junction angles can be modelled without much steric hindrance. Such junctional flexibility is compatible with the results of the limited proteolysis experiments done on sCD4[4].

The interface between protomers in the sCD4 dimer involves the D4 domains exclusively, and the buried surface (500 Å^2 from each non-hydrated protomer) is comparatively small, which suggests a relatively weak interaction. Although the operation that relates the protomers is non-crystallographic, it is within the bounds of error for a pure 2-fold axis ($\chi = 178.9°$ and $t_x = 0.37$ Å after the type-C refinement). Both the CC′ and FG loops of D4 protrude prominently from the C′CFG face of the β-sandwich[7] and the diad interface involves these features in a manner reminiscent of clasped hands.

Table 1 Diffraction data and refinement

Crystal type	Space group	Copy/ a.u.	Resolution (Å)	R_{merge}* (%)	Completeness* (%)	Reflections	Rigid body R/R_{free} (%)	Refinement R/R_{free} (%)
C	$P4_322$	2	8.0–3.9	11.2 (34.0)	80.0 (53.8)	11,993	41.2/42.5	24.0/35.1
F	P2	2	8.0–4.0	6.2 (25.4)	76.0 (45.8)	13,474	45.2/42.7	
A	$P3_121$	2	8.0–5.0	8.6 (29.5)	67.3 (49.9)	4,289	42.2/44.2	

* Numbers in parentheses indicate statistics for highest resolution shells.

Here, residues from the F and G strands together with those at the CC′ loop make direct contacts, and those at the FG loop may be close enough for water-mediated interactions (which cannot be modelled at this resolution). At the centre of the interface is a pair of absolutely conserved glutamine residues (Gln 344–Gln 344′) separated at hydrogen-bonding distance. All possible glycosylation sites known from CD4 sequences map outside the D4–D4′ interface (Fig. 1c) where they would neither interfere with nor participate in the dimer interaction. Although type-A crystals are in high salt and the C and F crystals are in low salt, all dimer interfaces are the same.

Given that dimers of sCD4 exist in these crystals, we have attempted to detect oligomerization of sCD4 in solution by way of ultracentrifugation, light scattering and chemical crosslinking. Ultracentrifugation of sCD4 showed it to be predominantly monomeric at 1 mg ml^{-1} (ref. 4); at higher sCD4 concentration (>5 mg ml^{-1}), however, non-ideal behaviour precluded satisfactory interpretation (P. Hensley, personal communication). Dynamic light-scattering measurements for D1D2 and sCD4 (1.25–20 mg ml^{-1}) showed that the apparent hydrodynamic radius was nearly concentration independent for D1D2 but increased by 46% for sCD4, and is well beyond extremes of concentration dependence seen for non-associating species. Treatment of sCD4 with glutaraldehyde produced dimer bands in a concentration-dependent manner, whereas only monomers were

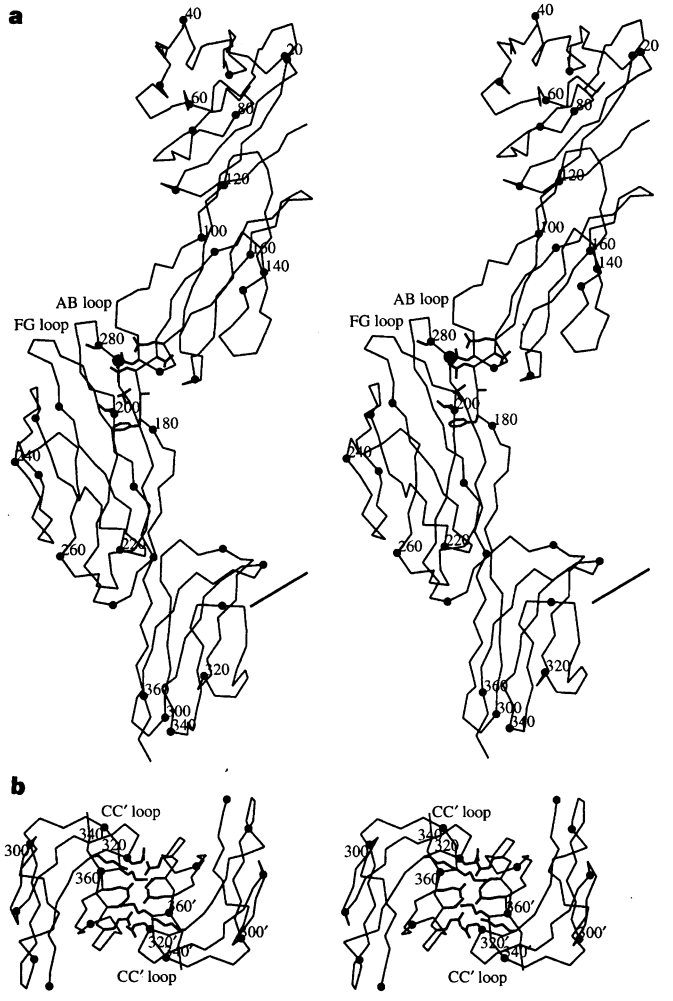

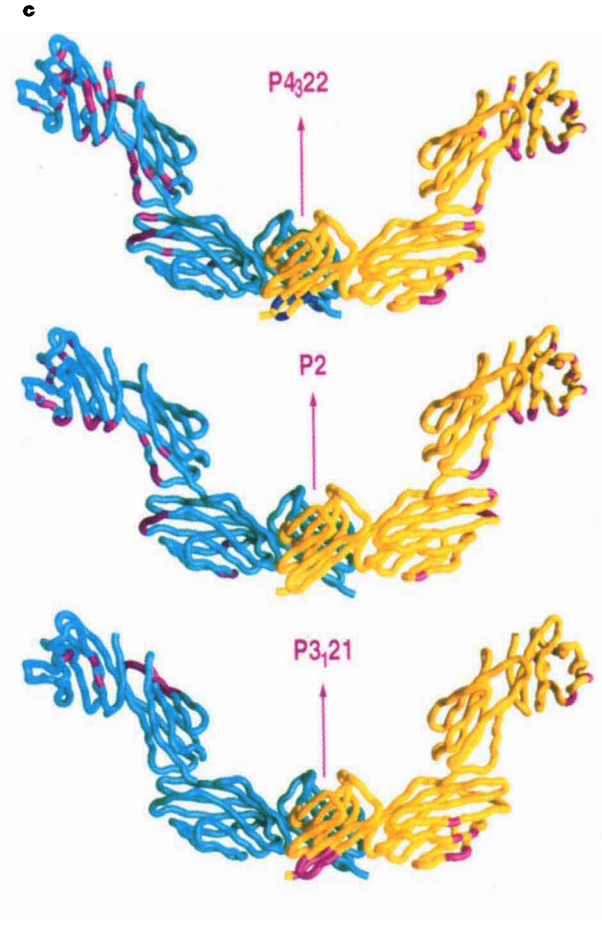

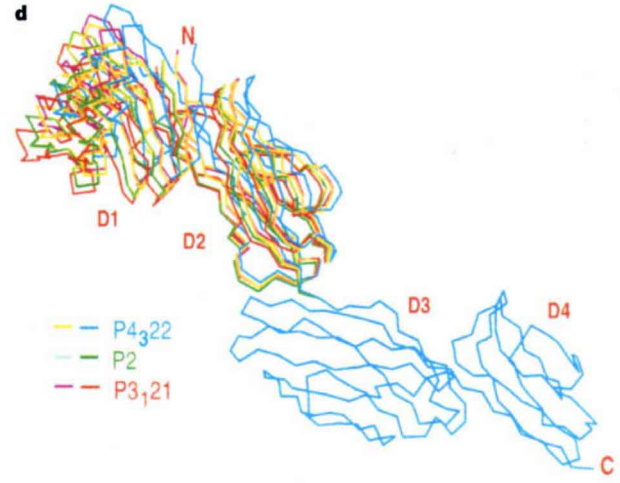

Figure 1 Structure of sCD4. **a**, Stereo C_α trace of D1–D4 (type-C, molecule 1). Every tenth residue is marked by a filled circle and every twentieth residue is labelled. Side chains are shown for those residues involved in the interaction between D2 and D3, including a larger filled circle for Gly 281. The dimer axis, 60° from the vertical, is indicated by a line. **b**, Stereo C_α trace of a D4–D4′ dimer (type C). The view is along the diad axis looking down at the hypothetical cell surface. Side chains are shown for residues at the dimer interface. **c**, Splined C_α traces of sCD4 dimers in three crystal forms. One protomer is in yellow and the other is in cyan. The diad axes are vertical. Footprints of lattice interactions, showing residues with at least one atom having a distance of less than 4.0 Å to an atom of neighbouring molecules, are in magenta. Potential glycosylation sites at the D4 domain for all the known CD4 sequences are dark blue on the tetragonal structure. **d**, Superposition of C_α traces to show flexibility at the D2 to D3 junction. The D2D4 domains of the six independent copies of sCD4 are superimposed, and each D1D2 domain is shown in a different colour. Pairwise relative rotations of the D1D2 domains are up to 10.4° and relative C_α displacements at the top of the CDR loops in D1 are up to 11.2 Å. **a** and **b** were produced with MOLSCRIPT[27]; **c**, with GRASP[28]; and **d**, SETOR[29].

evident in similar experiments with D1D2, even at the molar concentration equivalent to the highest sCD4 concentration (Fig. 2). Quantification of dimer formation as a function of protein concentration could be fitted with a K_D of 44.3 mg ml^{-1} (1.08 mM) (Fig. 2). No analogous dimer was observed in the crystal of rat D3D4[7], but the shorter construct of rat D3D4 (C terminus at residue 361, near the interface) may have interfered with dimerization. Moreover, with such low dimer affinity, dimers and monomers may coexist even under crystallization conditions so that favourable lattice contacts may compete successfully with the weak dimerization.

The crystalline sCD4 dimer is compatible with cellular assays of intact CD4 function for certain mutant variants. First, a mutational analysis of the interaction between CD4 and class II MHC found only one mutation outside domains D1 and D2 that had an effect[10]. This was located at residues 349–356 of human CD4, which overlap with the D4 dimer interface (Fig. 3). Second, an MHC-binding defective variant of CD4 (F43I) was shown to exert a dominant-negative effect on the ability of native CD4 to confer adherence to MHC-bearing cells and to boost T-cell activation, but only in the presence of its D3D4 domains, indicating oligomerization mediated by D3D4 (ref. 11). Moreover, the demonstration of two distinctive MHC sites for interaction with CD4 indicated the involvement of oligomerization of CD4 and/or class II molecules into ordered arrays[12]. Also, when the many point mutations in D1D2 that affect the MHC interaction[10,13–15] are mapped onto the sCD4 surface (Fig. 3), it appears that each protomer must interact with two different MHC molecules thereby yielding network formation.

The observed junctional flexibility also seems to have functional consequences, both in immune function and in HIV infection. Mutations at the hinge abolish the normal CD4 enhancement of interleukin-2 production[15]. Deletion of the flexible linker between D4 and the membrane[16] or binding of antibody Q425 near the D2 to D3 junction[17] both block HIV-mediated membrane fusion without affecting gp120 binding. Presumably, the demonstrated association of the membrane-distal CD4-gp120 complex with the membrane-embedded chemokine co-receptor[18,19] must require such flexibility.

CD4 is believed to increase the avidity of the TCR–MHC class II interaction which by itself would have typical lifetimes too short for effective signalling[1] and to contribute to signalling directly through its cytoplasmic association with Lck. The CD4–Lck association emulates a receptor tyrosine kinase, and we propose that ligand-induced dimerization[20] is the basis for signal transduction. In this case, the ligand is another cell. The C termini of the sCD4 dimer are 28 Å apart and project in parallel along the molecular diad. Kinase activation by *trans* autophosphorylation[21] could ensue when CD4 dimers form. When evenly distributed on a T-cell surface the CD4 level (we estimate approximately 10^{-5} M) would favour monomers, whereas during antigen recognition CD4 will be recruited by cooperative interactions to the adhesion junction[22] to a local concentration favouring dimers, especially when enhanced by the other interactions. In summary, the weak dimeric association of sCD4 seen first in the crystals and then confirmed in solution provides a basis for understanding signal transduction through CD4 in the cellular immune response. □

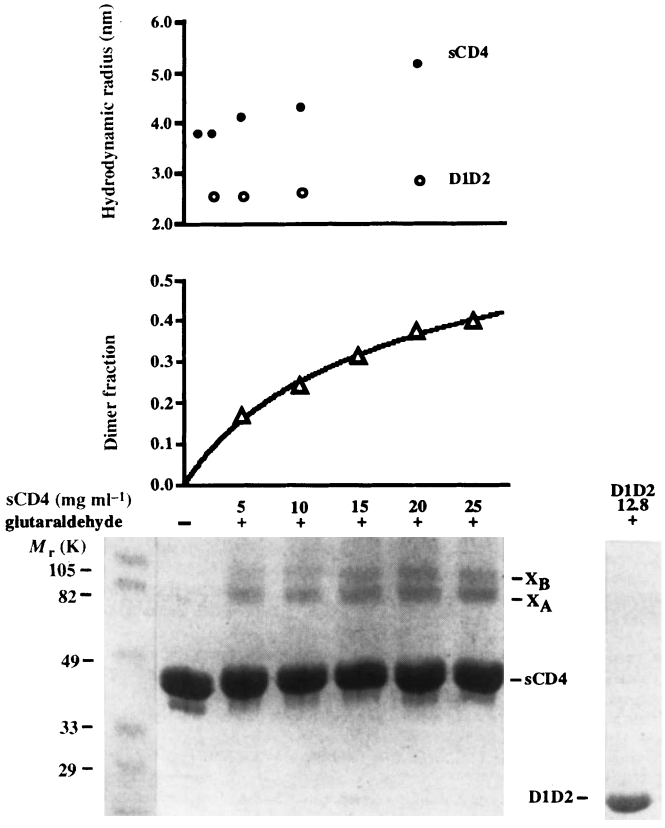

Figure 2 Solution experiments of sCD4. The top panel shows the apparent hydrodynamic radii as measured by dynamic light scattering of sCD4 (filled circles) at concentrations of 1.25, 2.5, 5.0, 10.0 and 20.0 mg ml^{-1} and of D1D2 (open circles) at concentrations of 2.5, 5.0, 10.0 and 20.0 mg ml^{-1}. The lower panels are results of crosslinking by glutaraldehyde. The SDS–PAGE gels contains molecular mass marker (lane 1), sCD4 (lane 2), sCD4 reacted with glutaraldehyde (lanes 3–7) with respective sCD4 concentrations of 5, 10, 15, 20 and 25 mg ml^{-1} and respective glutaraldehyde concentrations of 0.04, 0.08, 0.12, 0.16 and 0.20 mM, and D1D2 (lane 8) at 12.8 mg ml^{-1} reacted with 0.20 mM glutaraldehyde. Densities from the dimer bands as functions of protein concentrations were fitted to the dimerization equation with a single K_D (44.3 mg ml^{-1}) and a separate scale factor for each of the four repeated experiments. The average dimer fraction at each protein concentration is plotted together with the fitted curve. The r.m.s. residual in dimer fraction over the 20 independent observations was 0.02.

Methods

Protein preparation and crystallization. The expression, purification and crystallization of native sCD4 have been described earlier[4]. For selenomethionyl

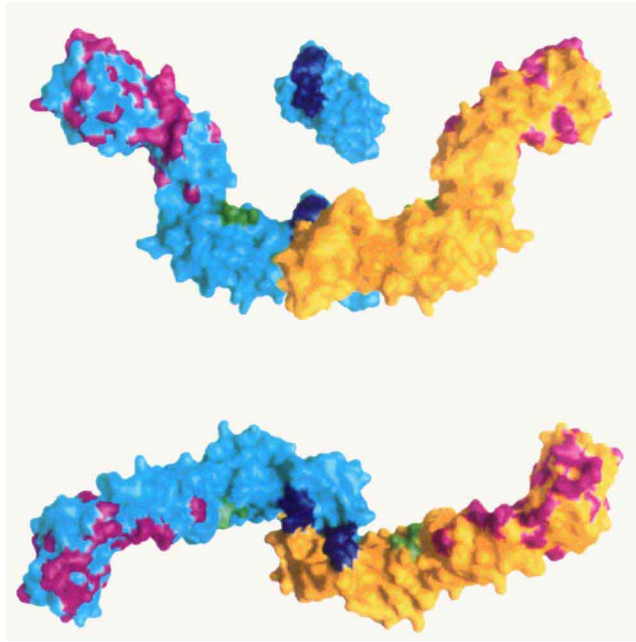

Figure 3 A summary of metagenesis data mapped onto the GRASP[28] surface of a sCD4 dimer. Solvent-exposed residues implicated in class II interaction by single-site mutations[10,13–15] are shown in magenta. Residues on D3 that may interact with TCR components are in green; when mutated these had an effect only when assayed in association with TCR[15]. The stretch of residues in D4 that may affect dimerization of CD4 is in dark blue[10]. Two orthogonal views are shown, and one D4 domain is 'pulled' away to show the dimer interface.

sCD4 production, confluent Chinese hamster ovary (CHO) cells were adapted for 2 days in methionine-free media (25 mM selenomethionine) and then incubated for 3 days in fresh media containing 250 mM selenomethionine. The secreted selenomethionyl sCD4 (80% incorporation by amino-acid analysis) was captured on S-sepharose and immunoaffinity purified with the Ca^{2+}-dependent anti-CD4 antibody Q425 (ref. 17). Under crystallization conditions for native type-D crystals (PEG 400, pH 8.7, 4 °C)[4], selenomethionyl crystals were obtained in the tetragonal type-C and the new monoclinic type-F lattices. To increase crystal size, sCD4 was pre-equilibrated for 4–5 days at 2/3 of the final PEG400 concentration (20%) in sitting-drop setups before dispensing into 4-μl hanging drops for final equilibrium. These crystals were directly cryoprotected in liquid propane. Type-A crystals were grown as before (ammonium phosphate, pH 8.7, 20 °C) from native sCD4 and used unfrozen. Cell dimensions for crystals used in the structure analyses are as follow: $a = b = 126.0$ Å and $c = 205.0$ Å for type A (trigonal); $a = b = 127.1$ Å and $c = 221.2$ Å for type C (tetragonal); and $a = 105$ Å, $b = 123.4$ Å, $c = 100.6$ Å, $\beta = 103.4°$ for type F (monoclinic). Cell dimensions for the type-F lattice are similar to those of the type-D lattice[4], but these crystals have a very different morphology and, using quantitative analysis[23] as well as structural verification, two rather than four monomers per asymmetric unit are found.

Structure determination. Diffraction data for selenomethionyl type-C and type-F crystals were collected at 110K at the peak of selenium K-shell absorption (0.9792 Å) on beamlines X25 and X4A, respectively, of the National Synchrotron Light Source. Data for native trigonal crystals in the type-A lattice were measured at room temperature at the F1 beam line of the Cornell High Energy Synchrotron Source. A combined molecular replacement procedure[8] was used first to solve the type-C structure. Two human D1D2 fragments[9] were located, then two D3 domains from the rat D3D4 model[7] (non-identical residues reduced to alanine) were found, and finally the D4 domains were included and refined by rigid-body adjustments. Non-crystallographic symmetry averaging was performed at 3.9 Å resolution with the DM program from the CCP4 suite followed by model building with O[24]. Residues 179–181 and 362–363 were added and the rat sequence of D3D4 was replaced by the correct human sequence to complete a model for residues 1–363. Refinement[25] proceeded with tight non-crystallographic restraints and R_{free} monitoring. The type-A and type-F crystals were solved by molecular replacement from the refined type-C model. Selenium Bijvoet-difference Fourier syntheses with model phases confirmed solutions for the C and F crystals; at least seven highest difference peaks corresponded to the expected eight selenium positions in each asymmetric unit.

Chemical crosslinking. Samples of sCD4 and D1D2 were reacted to completion (overnight) with glutaraldehyde at room temperature at constant molar ratios of protein to glutaraldehyde (3 : 1). The low glutaraldehyde concentration was chosen after a survey for conditions to prevent adventitious crosslinking at the higher concentrations of sCD4, D1D2 and bovine serum albumin (BSA). Each sample was denatured with 5% SDS and 2.5% β-mercaptoethanol, and a 3 μg aliquot was loaded and electrophoresed in 12.5% SDS polyacrylamide gel. Gels were stained by Coomassie blue and quantified with a densitometer. Staining is proportional to protein quantity within this range of densities. The crosslinking of sCD4 produced two higher molecular mass bands of approximately equal density that probably represent two possible linkage sites in an sCD4 dimer. The sCD4 model suggests two candidates for the observed species, one from Lys 360 to Lys 360′ and another from Lys 322 to Lys 188′, or vice versa; Nζ atoms for these pairs are close (<8.0 Å) and accessible. Crosslinking was not observable for the D1D2 or BSA samples.

Each lysine residue should have its own characteristic probability of initial reaction with glutaraldehyde, independent of sCD4 concentration. This should be unaffected by neighbouring reactions here, because sCD4 hits will be rare with 39 lysine residues per sCD4 and a 3 : 1 protein to glutaraldehyde ratio. In the event of reaction at a crosslinking site in the dimer, we presume that the second step, which is intramolecular, will be committed. Therefore, the abundance of crosslinked species is proportional to the dimer fraction in the sample. Based on a dimerization model of $A + A = A_2$, the fraction of dimers in a given concentration of total protein (c_T) is given by

$$y = 1 - \frac{K_D}{4c_T}\left(\sqrt{1 + \frac{8c_T}{K_D}} - 1\right)$$

where K_D is the dissociation constant. The dimer band density (D) is proportional to the dimer fraction, $D = S \times y$, where S is a scaling factor. A least-squares fitting of the $D(c_T)$ data give estimates of S and K_D.

Dynamic light scattering. Hydrodynamic radii of sCD4 and D1D2 at different concentrations were derived from dynamic light-scattering measurements[26] on a DynoPro Molecular Sizing Instrument (Protein Solutions, Inc.). Control experiments with BSA showed less than 6% variation over concentrations of 2.5–40 mg ml^{-1}.

Received 6 November 1996; accepted 26 March 1997.

1. Weiss, A. & Littman, D. R. Signal transduction by lymphocyte antigen receptors. *Cell* **76,** 263–274 (1994).
2. Lifson, J. D. & Engleman, E. G. Role of CD4 in normal immunity and HIV infection. *Immunol. Rev.* **109,** 93–117 (1989).
3. Deen, K. C. *et al.* A soluble form of CD4 (T4) protein inhibits AIDS virus infection. *Nature* **331,** 82–84 (1988).
4. Kwong, P. D. *et al.* Molecular characteristics of recombinant human CD4 as deduced from polymorphic crystals. *Proc. Natl Acad. Sci. USA* **87,** 6423–6427 (1990).
5. Ryu, S.-E. *et al.* Crystal structure of an HIV-binding recombinant fragment of human CD4 *Nature* **348,** 419–426 (1990).
6. Wang, J. *et al.* Atomic structure of a fragment of human CD4 containing two immunoglobulin-like domains. *Nature* **348** 411–418 (1990).
7. Brady, R. L. *et al.* Crystal structure of domains 3 and 4 of rat CD4: relation to the NH2-terminal domains. *Science* **260,** 979–983 (1993).
8. Tong, L. Combined molecular replacement. *Acta Crystallogr. A* **52,** 782–784 (1996).
9. Ryu, S.-E., Truneh, A., Sweet, R. W. & Hendrickson, W. A. Structures of an HIV and MHC binding fragment from human CD4 as refined in two crystal lattices. *Structure* **2,** 59–74 (1994).
10. Fleury, S. *et al.* Mutational analysis of the interaction between CD4 and class II MHC: class II antigen contact CD4 on a surface opposite the gp120-binding site. *Cell* **66,** 1037–1049 (1991).
11. Sakihama, T., Smolyar, A. & Reinherz, E. L. Oligomerization of CD4 is required for stable binding to class II major histocompatibility complex proteins but not for interaction with human immunodeficiency virus go120. *Proc. Natl Acad. Sci. USA* **92,** 6444–6448 (1995).
12. König, R., Shen, X. & Germain, R. N. Involvement of both major histocompatibility complex class II alpha and beta chains in CD4 function indicates a role for ordered oligomerization in T-cell activation. *J. Exp. Med.* **182,** 779–787 (1995).
13. Moebius, U. *et al.* Human immunodeficiency virus gp120 binding C′C″ ridge of CD4 domain 1 is also involved in interaction with class II major histocompatibility complex molecules. *Immunology* **89,** 12008–12012 (1992).
14. Moebius, U., Pallai, P., Harrison, S. C. & Reinherz, E. L. Delineation of an extended surface area on human CD4 involved in class II major histocompatibility complex binding. *Proc. Natl Acad. Sci. USA* **90,** 8259–8263 (1993).
15. Huang, G., Fleury, S., Yachou, A., Hendrickson, W. A. & Sekaly, R. Analysis of the contact sites on the CD4 molecule with class II MHC molecule: co-ligand versus co-receptor function. *J. Immunol.* **158,** 216–225 (1997).
16. Moir, S., Perreault, J. & Poulin, L. Postbinding events mediated by human immunodeficiency virus type I are sensitive to modifications in the D4-transmembrane linked region of CD4. *J. Virol.* **70,** 8019–8028 (1996).
17. Healey, D. *et al.* Novel anti-CD4 monoclonal antibodies separate human immunodeficiency virus infection and fusion of CD4+ cells from virus binding. *J. Exp. Med.* **172,** 1233–1242 (1990).
18. Lapham, C. K. *et al.* Evidence for cell-surface association between fusin and the CD4-gp120 complex in human cell lines. *Science* **274,** 602–605 (1996).
19. Wu, L. *et al.* CD4-induced interaction of primary HIV-1 gp120 glycoproteins with the chemokine receptor CCR-5. *Nature,* **384** 179–183 (1996).
20. Ullrich, A. & Schlessinger, J. Signal transduction by receptors with tyrosine kinase activity. *Cell* **61,** 203–212 (1990).
21. Yamaguchi, H. & Hendrickson, W. A. Structural basis for activation of human lymphocyte kinase lck upon tyrosine phosphorylation. *Nature* **384,** 484–489 (1996).
22. Kupfer, A., Singer, S. J., Janeway, C. A. & Swain, S. L. Coclustering of CD4 (L3T4) molecule with the T-cell receptor is induced by specific direct interaction of helper T cells and antigen-presenting cells. *Proc. Natl Acad. Sci. USA* **84,** 5888–5892 (1987).
23. Kwong, P. D., Pound, A. & Hendrickson, W. A. Volume-specific amino acid analysis: a method for Za determination. *J. Appl. Crystallogr.* **27,** 504–509 (1994).
24. Jones, T. A., Zou, J. Y., Cowan, S. W. & Kjeldgaard, M. Improved methods for building models in electron density maps and the location of errors in those models. *Acta Crystallogr. A* **47,** 110–119 (1991).
25. Brunger, A. T. *X-PLOR: A System for X-ray Crystallography and NMR* (Yale Univ. Press, New Haven, CT, 1992).
26. Harding, S. E. Determination of diffusion coefficients of biological macromolecules by dynamic light scattering. *Methods Mol. Biol.* **22,** 97–108 (1994).
27. Kraulis, P. MOLSCRIPT—a program to produce both detailed and schematic plots of protein structures. *J. Appl. Crystallogr.* **24,** 946–950 (1991).
28. Nicholls, A., Sharp, K. A. & Honig, B. Protein folding and association: insights from the interfacial and thermodynamic properties of hydrocarbons. *Proteins* **11,** 281–296 (1991).
29. Evans, S. V. SETOR: hardware-lighted three-dimensional solid model representations of macromolecules. *J. Mol. Graph.* **111,** 134–138 (1993).

Acknowledgements. We thank N. Belgado for tissue culture work; C. Ogata, L. Berman and M. Capel for assistance at beamlines; X. Zhao, H.-E. Aronson, Y. Liu and X. Zhu for help with the data collection; R. Bharadwaj for maintaining computer facilities; D. Snyder for help with dynamic light scattering; P. Hensley for ultracentrifugation attempts; and R. Sweet, R. Sekaly, L. Tong, and members of the Hendrickson laboratory for discussions. Synchrotron beamlines X4A and X25 at NSLS and F1 at CHESS are supported by the HHMI, DOE and NSF, respectively. The work was supported in part by an Aaron Diamond postdoctoral fellowship to H.W. and by grants from the National Institutes of Health and the Aaron Diamond Foundation. Atomic coordinates have been deposited in the Brookhaven Protein Data Bank (accession codes 1wio, 1wip and 1wiq).

Correspondence and requests for materials should be addressed to W.A.H. (e-mail hendw@convex.hhmi.columbia.edu).